



Article

Preparation of TiO₂ Nanoparticle Aggregates and Capsules by the ‘Two-Emulsion Method’

Nadya I. Politova-Brinkova, Sonya R. Tsibranska-Gyoreva, Slavka S. Tcholakova, Nikolai D. Denkov and Thomas Danner

Special Issue




Heterogeneous Interfacial Layers – Implications in Thin Liquid Films and Soft Colloids (Dedicated to the 65th Anniversary of Prof. Elena Mileva)

Edited by
Dr. Georgi G. Gochev



Article

Preparation of TiO₂ Nanoparticle Aggregates and Capsules by the ‘Two-Emulsion Method’

Nadya I. Politova-Brinkova ¹, Sonya R. Tsibranska-Gyoreva ¹, Slavka S. Tcholakova ^{1,*},
Nikolai D. Denkov ¹ and Thomas Danner ²

¹ Department of Chemical & Pharmaceutical Engineering, Faculty of Chemistry & Pharmacy, Sofia University, 1 J. Bourchier Ave., 1164 Sofia, Bulgaria; np@lcpe.uni-sofia.bg (N.I.P.-B.); st@lcpe.uni-sofia.bg (S.R.T.-G.); nd@lcpe.uni-sofia.bg (N.D.D.)

² BASF, GCT/P, L549, 67056 Ludwigshafen, Germany; thomas.danner@basf.com

* Correspondence: sc@lcpe.uni-sofia.bg; Tel.: +359-2-8161698

Received: 4 October 2020; Accepted: 30 November 2020; Published: 9 December 2020



Abstract: TiO₂-based materials are of great practical interest in several technological areas. Both the size and the morphology of the TiO₂ particles are of critical importance for their applications. The current study explores the effect of several factors on the outcome of the TiO₂ particle synthesis via the so-called ‘two-emulsion method’. In this technique, two water-in-oil emulsions—each of them containing different reactant in the dispersed water drops—are mixed under well controlled conditions. Upon such mixing, partial coalescence of the water drops from the two emulsions leads to mixing of the drop content, with chemical reaction occurring within the drops, and to synthesis of Ti(OH)₄ particles. Afterwards, the latter are transformed by emulsion heating into TiO₂ particles and aggregates of predominantly anatase structure. Our results show that—depending on the precursor and surfactant concentrations, oil viscosity, emulsification time, and mixing speed—the obtained nanoparticles could aggregate either on the drop surface, forming capsules with a very smooth surface, or inside the water droplets, thus leading to hierarchically structured aggregates of micrometer size. The spherical smooth capsules are constructed of very small monodisperse TiO₂ nanoparticles with size below 5 nm. The hierarchical bulk aggregates, on the other hand, are formed from bigger primary particles of sub-micrometer size. The obtained results show that one can obtain various TiO₂ structures by controlling the conditions during the emulsion preparation and mixing

Keywords: TiO₂ particles; nanoparticles; two-emulsion method; capsules; hierarchical structured aggregates

1. Introduction

TiO₂-based materials attract attention of the scientists for their potential and successful use in wide range of areas including photo-catalysis for self-cleaning of solid surfaces, water cleaning, in solar cells, sensors, memory devices, fillers, etc. [1–10]. Also, due to their high stability, non-toxicity, and bio-compatibility, TiO₂-based materials are used in implants and in drug delivery systems [11–14].

There are at least 11 reported bulk and/or nanocrystalline phases of TiO₂ and at least 3 reported non-crystalline TiO₂ phases [15–19]. The TiO₂ forms are constructed by Ti-O polyhedral, connected by a variable number of shared corners, edges, and/or faces. For the most common polymorphs of TiO₂—rutile, brookite, and anatase—the numbers of shared edges are, respectively, 2, 3, and 4 out of the 12 edges per octahedron [20]. The rutile and anatase are both tetragonal with distortion of the TiO₆ octahedron being larger for the anatase phase [21,22]. The brookite TiO₂ is orthorhombic, it has a larger cell volume and is not often used for experimental investigations [23]. The rutile is generally considered to be most stable under ambient conditions [24–26]. Hu et al. [27] have reported that TiO₂ normally

undergoes an anatase-to-rutile phase transformation in the range from 600–700 °C. This transformation was also affected by factors such as preparation conditions, precursors, impurities, and oxygen vacancies. Under high pressure, each of the phases—rutile, brookite, and anatase—transforms into II phase of TiO₂ [24,28,29]. The transformation sequence among the three main titania polymorphs (anatase, brookite, and rutile) is reported to be size dependent, because the energies of the three polymorphs are rather close and can be inverted by small differences in the surface energy [30]. If the particle size of the three nanocrystalline phases is equal, anatase is most thermodynamically stable at sizes < 11 nm, brookite is most stable for crystal sizes between 11 and 35 nm, and rutile is most stable at sizes > 35 nm [30].

Anatase is considered to show better photocatalytic activity compared to rutile [21,31], which is suggested to be due to the anatase's slightly higher Fermi level, lower capacity to adsorb oxygen, and higher degree of hydroxylation [31–34]. Some studies show that the mixture of anatase (70–75%) and rutile (30–25%) is more active than pure anatase [35,36]. However, other factors should be also considered, such as specific surface area, pore size distribution, crystal size, etc. Actually, a key parameter for the TiO₂ efficiency is the particle size and the experimental studies support the existence of an optimum particle size of TiO₂, at which, e.g., the photocatalytic oxidation rates of organic substrates are maximized. In some studies, this optimal size is claimed to be around and below 10 nm [37–39].

Various review papers summarize the methods for 0D, 1D, 2D and 3D TiO₂ material synthesis, properties and applications [2,8,40–44]. The list of the most used methods for preparation of TiO₂ nanoparticle includes hydrolytic [45–48] and non-hydrolytic [49,50] sol-gel method, bulk precipitation [51,52], hydrothermal and solvothermal methods [53–55], micellar and microemulsion methods [56–62], etc. Recently, some green methods for TiO₂ synthesis were reported [63,64]. In most cases, the authors use precursors that are typically inorganic salts (e.g., TiCl₄, Ti(SO₄)₂, or TiOSO₄) or titanium alkoxides (e.g., titanium isopropoxide or titanium butoxide) which hydrolyze in the presence of precipitation agents. As a result, different in size and morphology primary particles could be obtained in the range between 1 and above 100 nm. The particle growth was found to depend strongly on temperature, and also lowering the precursor concentration was shown to lead to a considerable decrease in the particle size [50]. The size, morphology and purity of the particles were also studied to depend on different parameters, such as the presence of different substances—amines [48], surfactants [51], and EDTA [52]—and on change of pH by addition of acids [58].

For efficient use of the obtained material, not only the size of the primary particles, but also the morphology of the formed aggregates is of critical importance. Actually, the size and the shape of the primary particles affects the morphology of the obtained aggregates. For example, very small particles, which pack together easily, are expected to form aggregates with smooth surfaces, while intermediate in size and big particles pack loosely and lead to the formation of structured aggregates. The latter may have some specific benefits, e.g., higher specific surface area, which makes them more appropriate as catalysts. For example, Boppella et al. [65] found better energy-conversion efficiency in the dye-sensitized solar-cells containing hierarchical TiO₂ structured aggregates compared with the commercial P25 TiO₂. The authors attributed the obtained better efficiency to the larger photon absorption by the increased path-length of the photons, due to multiple light scattering within the hierarchical TiO₂ aggregates [65]. Other structures are studied also in the literature, such as 3D TiO₂ nanotree arrays. Systematic review on the synthesis of such structures and their photovoltaic applications is presented by Wu et al. [8].

Recently TiO₂ micro- and nanospheres became the subject of very intensive studies due to their beneficial properties, such as low mass density, high specific surface area, better light absorption, efficient carrier separation, high durability, etc. [66–70]. Formation of TiO₂ aggregates in the form of smooth/hollow spheres or capsules could also have advantages in the industry, considering the advantages of both nanosized building blocks and the micron or submicron sized assemblies. For example, Ilaiyaraja et al. [71] showed increased performance for dye sensitized solar cells (DSSCs)

by fabricating composite photoanode via mixing larger TiO₂ microspheres with nanocrystallites, which allowed them to fill the voids between the larger particles [71].

The recent advances in the synthesis of nanostructured TiO₂ microspheres and their applications are discussed also in the reviews [72,73]. The most common methods for synthesis of such TiO₂ microspheres include the hard template methods, soft template methods or template-free methods [72]. Among these, the soft emulsion-drops-templated method appears to be very convenient, as it can provide different in size or uniform microspheres, depending on the emulsification conditions and on the size of the obtained emulsion drops. A limited number of studies are reported on that topic involving TiO₂ hollow spheres synthesis using normal or inverse emulsions [74,75]. In these studies, the obtained TiO₂ nano- and microspheres' size range is wide—between 50 nm and above 5 μm [74] or up to around 3 mm [75]. The authors showed that the use of inverse W/O emulsions for TiO₂ hollow spheres preparation (compared to direct O/W emulsions) leads to an increase of the monodispersity of the material and to reduction of the capsules' diameter by around 10 times and of their wall thickness by ca. 3 times [75]. The reported studies, however, were not focused on determination of the parameters which control the synthesis of the titania material.

Emulsion methods, and particularly the two-emulsion technique appeared to be successfully used for preparation of different nano- and microparticles (ZrO₂, CeO₂, Fe₂O₃, ZnS) [76–80]. However, it is not very easy to form stable inverse emulsions containing the precursors for the particles' synthesis in the droplets. There are also some restrictions like low drop fraction and low precursors concentration for formation of stable emulsions [76]. This leads to lower yield of the final synthesized material.

Despite the fact that the two-emulsion technique has been tested for particle synthesis, only a few papers are available for the use of this method for synthesis of TiO₂ nanomaterials. Most of the performed studies are in the field of microemulsions, that lead to formation of TiO₂ nanoparticles which, however, are not shown to aggregate in different desired structures than powder [61,81]. To the best of our knowledge, there are no studies in the literature focused on the controlled formation of TiO₂ structured aggregates of nanoparticles using the two-inverse-emulsion method. Therefore, a systematic study, which could provide information about the main parameters that are involved in the controllable synthesis of the TiO₂ nanomaterials by the two-emulsion methods, would be helpful to clarify the key factors and to provide guidelines for process optimization.

In the current study, we focused on the formation of TiO₂ nanoparticle materials of high concentration which aggregate in different structures, including spherical capsules with smooth or rough surface, or hierarchical aggregates using the two-emulsion method with inverse W/O emulsions, see Figure 1. The method includes the formation of two initial inverse emulsions with controllable stability, containing precursor-loaded water drops, which were then mixed under controlled stirring. As a result of the controlled drop-drop coalescence and subsequent emulsion heating, TiO₂ nanoparticles were formed which were aggregated in different structures. We studied the effect of the main factors which can be used for process control, incl. the surfactant and precursor concentrations, viscosity of the oily phase, and conditions during preparation and mixing of the precursor emulsions on the structure and morphology of the final TiO₂ material.

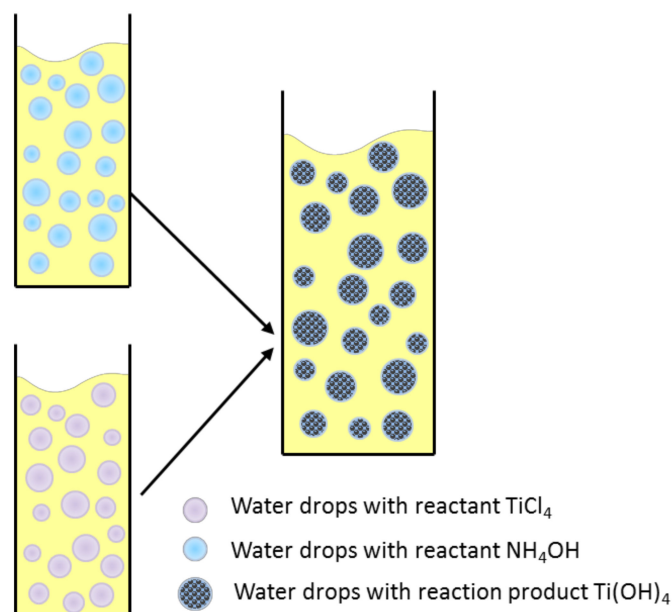


Figure 1. Schematic presentation of the two-emulsion method used in the current study for synthesis of TiO_2 particles and their aggregates. Two initial water-in-oil (W/O) emulsions, containing water drops with the reactants TiCl_4 and NH_4OH , are mixed and stirred under well controlled hydrodynamic conditions. During this stirring, the drop–drop coalescence leads to mixing of the reactants and to formation of Ti(OH)_4 as a reaction product inside the water drops which play the role of micro-reactors. The subsequent heating of the stirred emulsion transforms the Ti(OH)_4 into TiO_2 particles with predominantly anatase crystal structure.

2. Materials and Methods

2.1. Materials

We used TiCl_4 (product of Fluka, Radnor, PA, USA, cat.: 89541, purum $\geq 98.0\%$ (AT), molarity 8.94 M) as a precursor for TiO_2 synthesis, which we dissolved in concentrated HCl (32 wt %, molarity of 10.2 M HCl). As precipitation agent we used NH_4OH (25% ammonia water solution with technical purity, product of Teokom, Sofia, Bulgaria, molarity of 13.36 M).

When preparing the emulsions we tested two different types of oils with different viscosities: hexadecane (chemical formula $\text{C}_{16}\text{H}_{34}$, product of Alfa Aesar, Haverhill, MA, USA, 95% purity, cat.: 43283, mass density of 0.7733 g/mL) with $\eta = 3 \text{ mPa}\cdot\text{s}$ ($T = 20 \text{ }^\circ\text{C}$) and Heavy oil (product of Sigma-Aldrich, St. Louis, MO, USA, cat.: 33,076-0, mass density of 0.862 g/mL) with $\eta = 130 \text{ mPa}\cdot\text{s}$ ($T = 20 \text{ }^\circ\text{C}$).

For determination of appropriate surfactant for stabilization of the water-in-oil (W/O) emulsions, we tested different nonionic surfactants as emulsifiers: Lutensols A8, TO8 and TO2 (fatty- or oxoalcohol ethoxilates with chemical formula $\text{C}_{12-18}(\text{EO})_x$, products of BASF, Ludwigshafen, Germany), Brij 30 (polyoxyethylene-4-lauryl ether, product of Sigma), Brij 52 (polyoxyethylene-2-cetyl ether, product of Aldrich), Brij 72 (polyoxyethylene-2-stearyl ether, product of Sigma), Span 20 (sorbitan monolaurate, NF, product of ICI, London, UK), Span 40 (sorbitan monopalmitate, chemical formula $\text{C}_{22}\text{H}_{42}\text{O}_6$, product of Merck, Darmstadt, Germany), Span 60 (sorbitan monostearate, product of Rhodia, La Défense, France), Span 65 (sorbitan tristearate, product of Merck, Darmstadt, Germany), and Span 80 ($\text{C}_{24}\text{H}_{44}\text{O}_6$, sorbitan monooleate, product of Fluka, USA). These surfactants, along with their type and HLB values, are described in Table S1 in the Supporting Information.

Note that TiCl_4 is classified as corrosive and reactive substance. Therefore, we used the necessary safety procedures. All experiments with TiCl_4 were performed in a well-ventilated chemical fume hood with high caution. The operators were equipped with chemical protective clothing (Dupont,

Wilmington, DE, USA, Tyvek Classic model CHF5 Type 5 and 6 with hood, category III), half mask respirator (3M[®], St. Paul, MN, USA, 6000 series) with respiratory Gas filter (3M[®], ABEK1, 6059), chemical goggles, gloves (Kimtech Science, Irving, TX, USA, Purple Nitrile), and protective shoes. After the experiments, all TiCl₄ residues on the used materials (beakers, syringes, needles, pipettes, etc.) were neutralized using Ca(OH)₂ before disposal.

2.2. Methods and Procedures

2.2.1. Two-Emulsion Method

To obtain TiO₂ we performed the reaction of preparation of Ti(OH)₄, see Equation (1), which then transformed into TiO₂ under heating.



As the reaction takes place inside the drops of W/O emulsion, Figure 1, these drops essentially play the role of micro-reactors for synthesis of the desired Ti(OH)₄ and TiO₂ particles. The Ti(OH)₄ containing emulsion was prepared by mixing two initial W/O emulsions, containing the precursor chemicals, TiCl₄ (TiCl₄-emulsion) and NH₄OH (NH₄OH-emulsion). The aqueous phase of the first emulsion was an 8.94 M solution of TiCl₄ in concentrated 10.2 M solution (32 wt %) of HCl acid. The aqueous phase of the other initial emulsion was 13.4 M solution (25 wt %) of NH₄OH in water. The coalescence of the drops after mixing these two initial emulsions led to the formation of Ti(OH)₄ which was then transformed into TiO₂ after heating the mixed emulsion at 100 °C for 30 min in oil bath, under continuous stirring on a magnetic stirrer.

Most of the experiments were performed using the following procedure:

- (1) A water–oil premix of each initial emulsion was prepared by addition of the necessary amount of water phase in the oily phase under continuous stirring to form coarse emulsion. To form the premix we first prepared the oily phase which consisted of Span 80 (in the concentration range between 0.1 and 3 wt % with respect to the oily phase of the emulsion) dissolved in 24 g of the oil (hexadecane or heavy oil) at room temperature on a magnetic stirrer. The volume of the aqueous phase of the NH₄OH-emulsion was 6.3 mL. The aqueous phase of the TiCl₄-emulsion, containing 8.94 M TiCl₄, was prepared by dissolving 1.67 mL TiCl₄ into 4.03 mL concentrated 10.2 M HCl. The addition was performed dropwise on a magnetic stirrer in an ice bath. Due to the decrease of the solution volume during mixing (by a factor of 1.23 ± 0.01), the obtained final volume of the TiCl₄ + HCl solution was 4.63 mL.
- (2) The water volume fraction of the NH₄OH-emulsion was 17 vol % when working with hexadecane and 18 vol % when working with heavy oil. With account of the decrease of the volume upon mixing of TiCl₄ and HCl in the aqueous phase, we calculated the water volume fraction of the respective initial TiCl₄-emulsions to be 13 vol % when working with hexadecane and 14 vol % when working with heavy oil.
- (3) Rotor-stator emulsification device Ultra Turrax (Janke & Kunkel GmbH & Co, IKA-Labortechnik, Germany) was used for homogenization of the two W/O premixes in order to obtain the two initial emulsions. The homogenization time was set to 5 min. The rotation speed of the homogenizing element was fixed at 8000; 13,500; or 20,500 rpm in the various experiments, all performed at room temperature.
- (4) The NH₄OH-emulsion was then added to the TiCl₄-emulsion under mild stirring. Next, we homogenized the mixed emulsion with Ultra Turrax to realize drop-drop coalescence under well-defined conditions and, thus, to trigger the reaction leading to Ti(OH)₄ precipitation. In these series of experiments, we varied systematically the homogenization time (10, 15, 20, 30, or 40 min) and

the rotation speed (8000; 13,500; 20,500 rpm). The average concentrations of the reactants with respect to the water phase in the mixed emulsions were calculated to be 1.37 M for TiCl_4 , 3.75 M for HCl, and 7.7 M for NH_4OH . Note that, along with the formed $\text{Ti}(\text{OH})_4$ precipitate, about 7.7 M NH_4Cl is formed in the aqueous phase as a reaction byproduct, see Equation (1).

- (5) Finally, the mixed emulsion was heated at 100 °C for 30 min under stirring on a magnetic stirrer for $\text{Ti}(\text{OH})_4$ transformation into TiO_2 . In this way, we obtained W/O emulsion with water volume fraction of $\approx 15\%$ using hexadecane as the oily phase and $\approx 16\%$ using heavy oil, with about 11 wt % of TiO_2 particles and agglomerates residing in the aqueous drops.

To study the effect of the precursor concentration, some of the experiments were performed using the same procedure, but at lower precursor concentration of about 0.66 M TiCl_4 which led to lower TiO_2 and NH_4Cl concentrations in the final emulsion.

2.2.2. Determination of Drop Size Distribution

The drop size distribution in the obtained emulsions was determined by video-enhanced optical microscopy. The oil drops were observed and recorded in transmitted light with microscope Axioplan (Zeiss, Oberkochen, Germany), equipped with objective Epiplan $\times 50$, and connected to CCD camera and DVD recorder. The diameters of the recorded water drops were measured by operator, with custom-made image analysis software. Each droplet was measured individually by the operator. For each sample, the diameters of at least 1000 drops were measured. The characteristic average volume-surface diameter, d_{32} , was determined from the measured drop diameters. It is defined as

$$d_{32} = \left(\sum_i N_i d_i^3 \right) / \left(\sum_i N_i d_i^2 \right) \quad (3)$$

where N_i is the number of drops with diameter d_i in the sample analyzed.

2.2.3. Particle Separation

The formed TiO_2 particles inside the emulsion droplets had to be separated both from the oily phase and from the byproduct (NH_4Cl). We used the following protocol for this separation. After completing the emulsion stirring and heating, the particles and the water droplets were left to sediment and the oily phase above them was removed. Three-fold dilution of the aqueous sediment with HCl of pH = 1 was applied and, then, the pH was raised to ≈ 6 by addition of 13.4 M NH_4OH to break the W/O emulsion and to aggregate (weakly) the TiO_2 particles in the aqueous phase for their easier washing and separation. Multiple particle washing with H_2O was performed afterwards. Finally, the particles were centrifuged at 1000 g for 30 min to remove the water phase and were re-dispersed in HCl with pH = 1 (re-dispersed particles), or the particles were dried at 120 °C for 1–2 h (dried particles) for further analysis.

2.2.4. Analysis of the Particles

Dynamic Light Scattering (DLS) Analysis

The size of the obtained TiO_2 particles was measured by Dynamic Light Scattering (DLS) method at 25 °C \pm 0.1 °C, using apparatus Malvern 4700 (Malvern Ltd., Leamington Spa, UK). The light source was a laser operating at 532 nm wavelength. For this purpose, the dispersion of TiO_2 particles, obtained as explained in Section 2.2.3, was diluted in HCl with pH = 1 until slightly opalescent sample, suitable for DLS analysis, was achieved. Sonication in ultrasonic bath for 15–20 min was applied just before the DLS measurements to disperse the particle agglomerates formed in the preceding procedures.

For measuring the size of the dried particles (see Section 2.2.3), we prepared the DLS sample by re-dispersing a small amount of the dried particles in 30 mL HCl with pH = 1. This sample was sonicated in ultrasonic bath for 20–30 min and with a pulse sonicator for 2 min (SKL650-IIDN, Ningbo

haishu sklon develop co., Ltd., Zhejiang, China) to break the particle agglomerates. The sonicator was set to work at 450 W and 1 s long pulses with 0.5 s off period were applied (recommended by manufacturer). A sonotrode with a diameter of 3 mm was used for the sonication.

Scanning Electron Microscopy (SEM) and Elemental Analysis (EDX)

We performed also SEM and EDX analysis of the samples using SEM/FIB LYRA I XMU (TESCAN, Brno, Czech Republic) equipped with EDX detector Quantax 200 (BRUKER, Billerica, MA, USA), Spectroscopic resolution at Mn-K α and 1 kcps 126 eV, LN-free. We used SE detector and worked at 5–30 keV. We analyzed the powder of dried particles which was covered with carbon just before analysis.

X-ray Analysis

We performed X-ray analysis for some of the samples to determine the crystal structure of the obtained particles. Powder of dried particles was analyzed. Wide-angle diffraction data were collected on a diffractometer D500 (Siemens, Munich, Germany) using CuK α radiation and a secondary beam graphite monochromator. The spectra were recorded in the 2 theta range from 20° to 60°, in steps of 0.05° and counting time of 2 s/step.

Transmission Electron Microscopy (TEM)

TEM analysis of the samples was performed using high resolution TEM (HRTEM) JEOL JEM 2100, operated at 200 kV. The magnification was in the range of $\times 40,000$ to $\times 400,000$. For sample preparation we used the particle dispersions in HCl with pH = 1, obtained as described in Section 2.2.3. Before analysis, these samples were sonicated in an ultrasonic bath for 3–5 min. Then a drop from the particle dispersion was placed on a regular Cu grid for TEM observations, covered with amorphous carbon. Before the observations by TEM, the grids were dried for 24 h at room temperature, in air at atmospheric pressure.

3. Results and Discussion

3.1. Selection of Appropriate Emulsifier for Stabilization of Water-in-Oil Emulsions with Controllable Stability

The preparation of inverse water-in-oil (W/O) emulsions with controllable stability is not an easy task, especially in the presence of reagents like TiCl $_4$ + HCl or NH $_4$ OH of high concentration in the aqueous phase. Our aim in this part of the study was to select suitable emulsifiers that stabilize the initial W/O emulsions upon storage, but allow drop-drop coalescence upon stirring of the mixed emulsions, initially containing the two precursors in separate water drops. With this aim in view, we tested surfactants from the Lutensols, Brij, and Spans series as emulsifiers. As a continuous phase, we tested two oils with different viscosities: hexadecane ($\eta = 3$ mPa·s) and heavy mineral oil ($\eta = 130$ mPa·s).

First, experiments using deionized water as aqueous phase and hexadecane as a continuous phase were performed. The water volume fraction was 20% and the concentration of the surfactant was fixed at 1 wt %. All emulsions in this part of the study were prepared with Ultra Turrax at homogenization time of 5 min and rotation speed of 13,500 rpm. The results showed that only Brij 72 from the group of Lutensol and Brij series was able to support the formation of W/O emulsions. However, these emulsions were unstable—separation of the oil and water phases occurred within 1 min after stopping the emulsification.

The results with surfactants from the Span group showed that stable W/O emulsions are formed when Span 20 or Span 80 are used as emulsifiers at room temperature, and Span 60 can be used if the emulsification is made at 60 °C. The emulsification conditions were the same as those described above for the surfactants in the Lutensol and Brij groups. Thus, for the further experiments we selected Span 20 and Span 80 which give stable W/O emulsions when used at sufficiently high concentrations.

For the latter two surfactants, we tested how the emulsion stability depends on the emulsifier concentration. Emulsion stability was characterized by measuring the time required to obtain clear water phase (separated due to coalescence of the water drops in the emulsion) on the bottom of the container. The obtained results are presented in Figure 2. One sees that Span 80 stabilizes W/O emulsions even at 0.1 wt %, whereas 10-times higher concentration is needed when Span 20 is used as emulsifier. Therefore, the most appropriate surfactant for formation of relatively stable emulsions of this kind is Span 80 at concentrations ≥ 0.1 wt %.

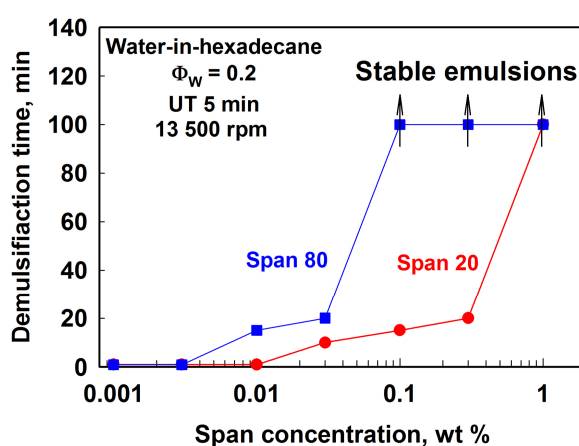


Figure 2. Demulsification time as a function of the weight concentration of the surfactants Span 20 and Span 80 for 20 vol % emulsions of water-in-hexadecane. The emulsification procedure was performed with Ultra Turrax rotor-stator homogenizer for 5 min at 13,500 rpm.

Further experiments showed that Span 80 successfully stabilizes W/O emulsions with composition of the aqueous phase $\text{TiCl}_4 + \text{HCl}$, or NH_4OH when hexadecane or heavy oil are used as oily phase. Therefore, Span 80 is used in all experiments described below.

3.2. Synthesis of TiO_2 Particles and Analysis of the Obtained Structures

Series of experiments were performed varying the concentrations of the emulsifier and the precursor, the oil type and the conditions upon mixing of the two initial emulsions.

3.2.1. Effect of Emulsifier Concentration

First, we performed experiments varying the emulsifier concentration in emulsions containing hexadecane as oily phase. The average concentration of the precursor with respect to the aqueous phase of the mixed emulsion was ≈ 1.37 M TiCl_4 . The emulsion preparation was performed with Ultra Turrax for 5 min at 13,500 rpm, while for the emulsion mixing we used the same rotation speed for 10 min.

The SEM analysis of the final TiO_2 samples dried at 120°C (Section 2.2.3) showed non-trivial shapes of the TiO_2 aggregates, depending on the surfactant concentration: either bulky agglomerates with rough surface or spherical capsules with very smooth surface were observed, see Figure 3. The procedure analysis suggested that the morphology of the obtained TiO_2 agglomerates is determined mostly by the size of the primary TiO_2 particles.

Therefore, next we studied the size and the morphology of the primary particles in the non-dried TiO_2 dispersions using TEM, see Figure 4. In all these samples we observed very small primary particles within the range of 1–5 nm. However, in the samples obtained at lower surfactant concentration bigger primary particles and their aggregates were observed along with the small ones as illustrated in Figure 4a. These bigger particles were not observed at high Span 80 concentrations, Figure 4c. This difference reflects the rate of coalescence during the emulsification process.

At the lowest surfactant concentration of 0.1 wt, very intensive coalescence occurs between the aqueous drops in the stirred emulsion which leads to the formation of bigger primary particles. These bigger particles then aggregate to form bulky structured agglomerates with rough surface after drying at 120 °C (Figure 3a,b).

The increase of the Span 80 concentration up to 1 wt % or higher, suppresses such uncontrollable coalescence during emulsion stirring, thus providing restricted volume for particles synthesis inside the individual emulsion drops. The nucleation of particles in such limited volume ended up into the formation of very small primary particles which pack closely during aggregation, forming spherical capsules with very smooth surface after drying at 120 °C. These observations show also that these small TiO₂ nanoparticles aggregate on the surface of the emulsion drops, similarly to the soft-template methods for synthesis of TiO₂ spheres [74,75].

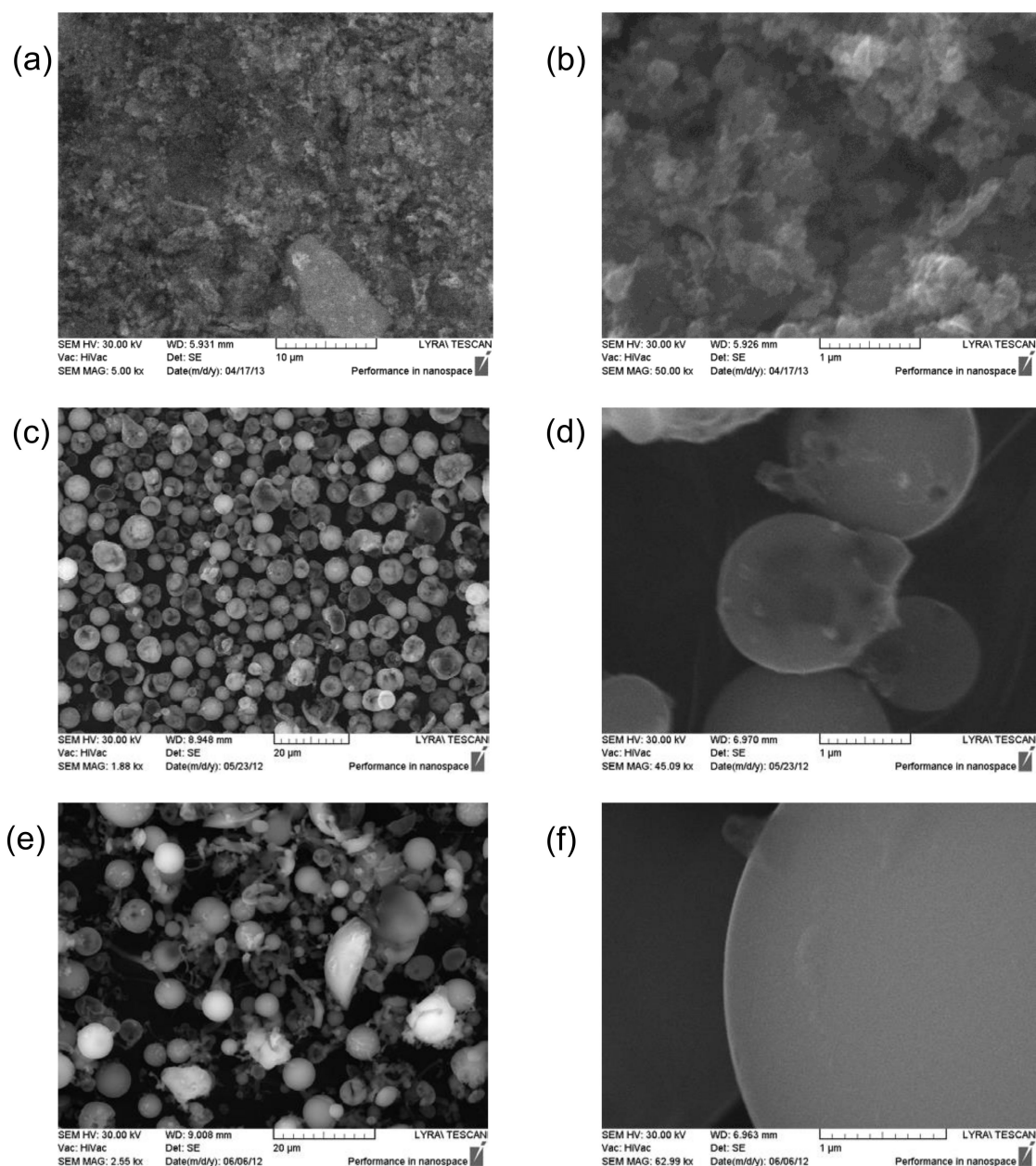


Figure 3. SEM images of particle aggregates obtained at precursor concentration of 1.37 M TiCl₄ and oily phase containing (a,b) 0.1 wt % Span 80, (c,d) 1 wt % Span 80, or (e,f) 3 wt % Span 80 dissolved in hexadecane.

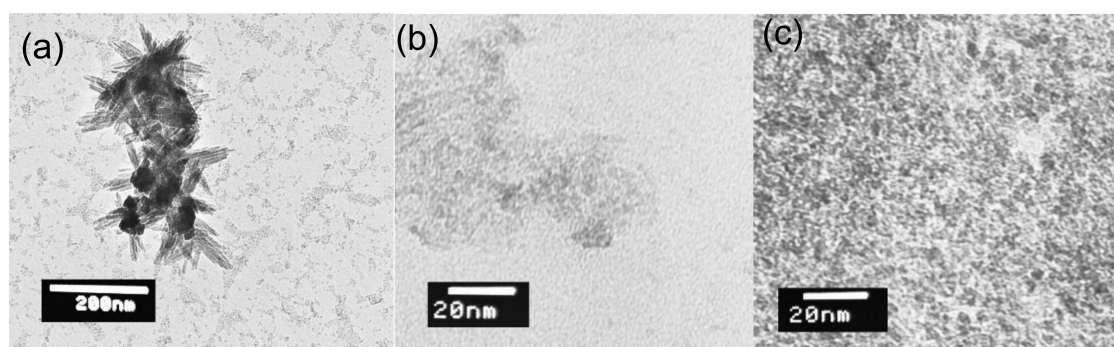


Figure 4. TEM images of the primary particles and their aggregates obtained at precursor concentration of 1.37 M TiCl_4 and oily phase containing Span 80 of concentration (a) 0.1 wt %, (b) 1 wt %, or (c) 3 wt % in hexadecane.

The fact that the primary particles could be observed by TEM analysis shows that the obtained aggregates could be easily destroyed upon sonication if no pre-drying was applied. Upon drying at 120 °C, however, strong adhesive forces arise and keep the primary particles fixed in aggregates which are hard to destroy.

The size of the formed particles aggregates was measured by DLS to clarify the effect of surfactant concentration in the emulsions and the role of particle drying. DLS measurements just after particles synthesis in the TiO_2 dispersions (before their drying) and after drying of the particles at 120 °C were performed and the results are summarized in Figure S1 in the Supporting Information. The results for the samples after drying corresponded well to the sizes of the aggregates observed in the SEM analysis—the average agglomerate size increased with the increase of surfactant concentration. On the other hand, much smaller aggregates in the submicrometer range were measured in the respective samples before their drying. In other words, the bulky agglomerates and the spherical capsules can be destroyed upon sonication if the samples are not dried at high temperature.

3.2.2. Effect of the Oily Phase

We studied the role of the oily phase using two oils with very different viscosities—hexadecane and heavy oil. In all experiments presented in this section, the concentration of the surfactant was 1 wt % Span 80 and the concentration of the precursor with respect to the aqueous phase in the mixed emulsions was 1.37 M TiCl_4 . The emulsification was performed by Ultra Turrax at 20,500 rpm for 5 min, whereas the emulsion mixing and stirring was for 10 min at the same rotation speed.

The results showed significant difference in the aggregation of the particles after drying, depending of the used oil. The emulsification with hexadecane led to the formation of spherical capsules, Figure 3c,d, while bulky agglomerates of micrometer size were formed in the emulsions with heavy oil, Figure 5a. These results indicate that the small primary particles aggregate on the surface of the emulsion drops in the experiments with hexadecane. In contrast, the primary particles aggregate in the interior of the emulsion drops in the systems with heavy oil. TEM analysis showed also the formation of bigger TiO_2 particles with size of 100–200 nm in the emulsions prepared with heavy oil, along with the very small nanoparticles (with size in the range of several nm), observed with hexadecane emulsions at high surfactant concentration, Figure 5b.

The increase of the oil viscosity, however, seems to diminish the effect of drying on the final aggregates' sizes, as evidenced by comparing the DLS results from samples prepared with hexadecane and heavy oil, before and after drying at 120 °C. The aggregates formed inside the emulsion droplets and containing bigger TiO_2 particles in heavy oil emulsions are more prone to be destroyed upon sonication when compared to the strongly aggregated spherical capsules obtained from very small nanoparticles in hexadecane emulsions, Figure S2 in Supporting Information.

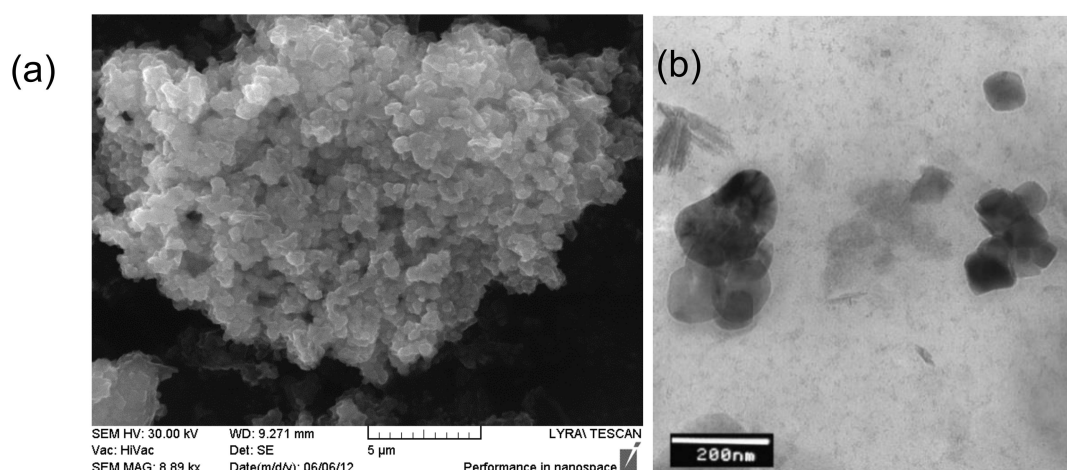


Figure 5. (a) SEM image of aggregates and (b) TEM image of primary particles forming these aggregates, obtained with 1 wt % Span 80 in heavy oil. The precursor concentration was 1.37 M TiCl_4 .

3.2.3. Effect of the Precursor Concentration

To study the effect of precursor concentration on the particle formation and aggregation, we performed experiments at reduced concentration of $\text{TiCl}_4 \approx 0.66$ M (with respect to the aqueous phase in the mixed emulsions). Results showed that such two-fold decrease of the precursor concentration diminishes the effect of oil viscosity. SEM images of the samples at the lower precursor concentration in hexadecane emulsions showed no longer spherical but mostly structured aggregates, similar to those observed in heavy oil emulsions, Figure 6. The formed primary particles are bigger at lower precursor concentration in hexadecane emulsions. Also, the particle aggregation in this case occurs probably in the drop interiors, not on the drop surface. The latter process could be related to the different concentrations of the byproduct, NH_4Cl , formed in different quantities at high and at low precursor concentrations, respectively. For reasons which are not very clear at the moment, the decrease of the precursor and of the byproduct concentrations resulted in bigger primary particles, as shown in Figure 7, which could not pack closely and result in hierarchical aggregates after drying, Figure 6.

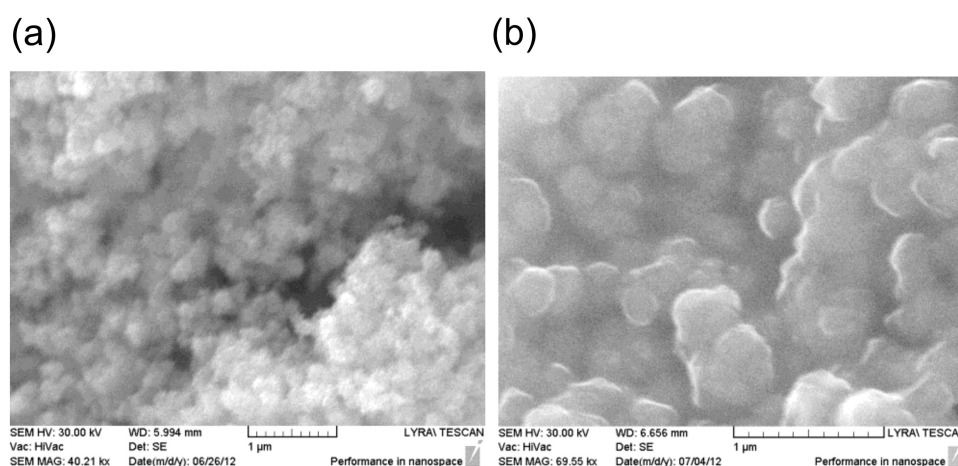


Figure 6. SEM images of particle aggregates obtained at precursor concentration of about 0.66 M TiCl_4 and surfactant concentration of 1 wt % Span 80 in (a) hexadecane and (b) heavy oil.

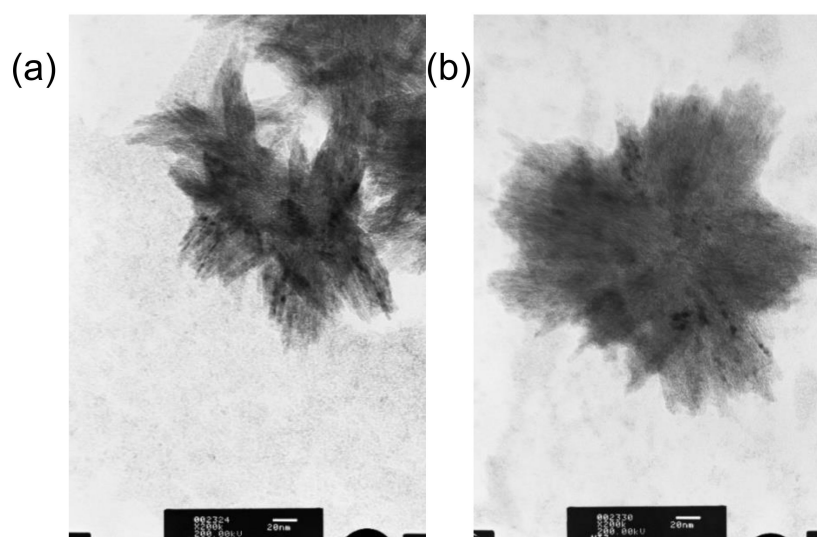


Figure 7. TEM images of the particles obtained with 0.66 M TiCl_4 and surfactant concentration of 1 wt % Span 80 in (a) hexadecane and (b) heavy oil.

The DLS measurements showed also that using precursor of lower concentration leads to aggregates which could be destroyed by sonication—sizes in the submicrometer range were measured for the dried samples obtained with 0.66 M TiCl_4 . These trends are illustrated in Table 1 which summarizes the average aggregate sizes measured by DLS before and after drying at 120 °C for the particles obtained with hexadecane and heavy oil, at the two precursor concentrations. No significant difference is seen at 0.66 M TiCl_4 when working with hexadecane or heavy oil, which was not the case at the higher precursor concentration. The difference before and after drying is also not very significant with hexadecane emulsions at 0.66 M TiCl_4 , in contrast to the results obtained with 1.37 M TiCl_4 .

Table 1. Particle aggregate sizes represented as mean diameter by number, d_N , and by volume, d_V , as measured by DLS at different concentrations of the TiCl_4 precursor, after particle synthesis in emulsions formed in hexadecane or heavy oil. The Span 80 concentration in the oily phase was 1 wt % in all these experiments. The preparation of the initial emulsions was performed with Ultra Turrax at 20,500 rpm for 5 min, whereas the mixing of these emulsions was made for 10 min at the same rotation speed.

TiCl_4 , M	Hexadecane				Heavy Oil			
	Before Drying		After Drying		Before Drying		After Drying	
	d_N , nm	d_V , nm	d_N , nm	d_V , nm	d_N , nm	d_V , nm	d_N , nm	d_V , nm
0.66	430	520	430	900	420	500	420	900
1.37	240	390	430	5000	420	500	420	660

3.2.4. Effect of Emulsification Conditions—Homogenization Time and RPM

To clarify the effect of the homogenization conditions, we performed emulsification experiments varying the homogenization time at fixed rotation speed and, alternatively, at different rotation speeds at fixed homogenization time.

The results from the DLS measurements of the particle aggregates formed at different homogenization times are compared in Figure S3 in the Supporting Information. These results show that the increase of the homogenization time of the mixed emulsions from 10 to about 15 or 20 min leads to significant decrease in the measured size of the aggregates.

We also studied the effect of the different rotation speeds during the formation of the initial emulsions and during the emulsion mixing and stirring. Illustrative results for the morphology of the obtained aggregates are shown in Figure 8. These images are for samples, obtained at high precursor concentration of 1.37 M TiCl_4 and with 1 wt % Span 80 dissolved in hexadecane as oily phase. One sees that the changes in the homogenization speed affect the size of the primary particles and the surface roughness of the formed aggregates. The morphology of these aggregates reflects the size and the shape of the primary particles shown in Figure 9. The comparison of the images in Figures 8 and 9 shows that aggregates with rough surface are obtained from bigger primary particles, while the aggregates with smoother surface are formed from much smaller and well-packed primary particles.

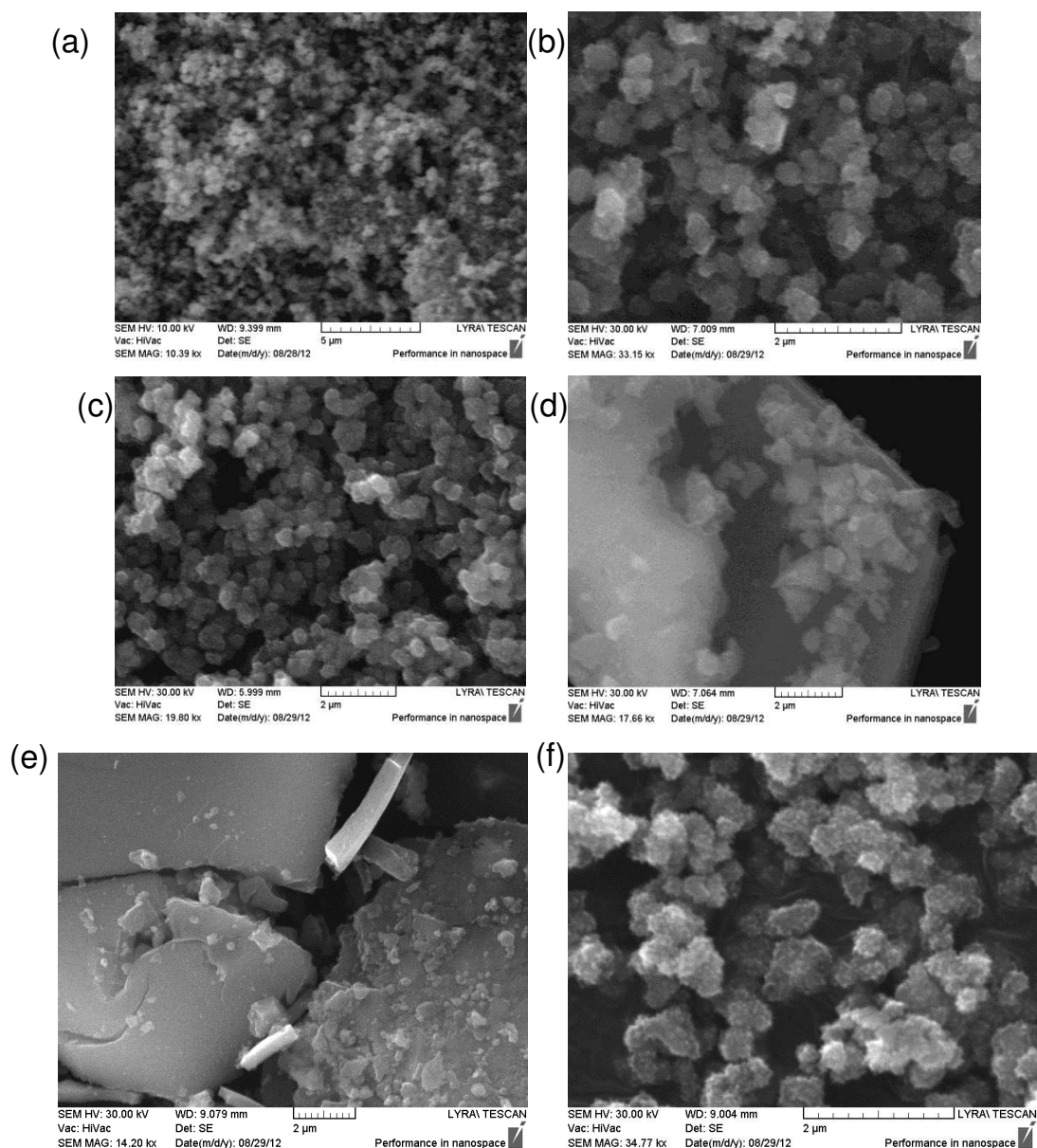


Figure 8. SEM images of the formed aggregates from TiO_2 particles at ≈ 1.37 M concentration of the precursor TiCl_4 (with respect to the aqueous phase) and 1 wt % surfactant Span 80 (with respect to the oil) in hexadecane. The emulsification was performed with Ultra Turrax. In cases (a–c) the initial emulsions were prepared at 20,500 rpm for 5 min and the emulsion mixing was made at (a) 8000 rpm, (b) 13,500 rpm, and (c) 20,500 rpm for 10 min. In cases (d–f) the initial emulsions were obtained at (d) 8000 rpm, (e) 13,500 rpm, and (f) 20,500 rpm and the mixing was made at 20,500 rpm for 10 min.

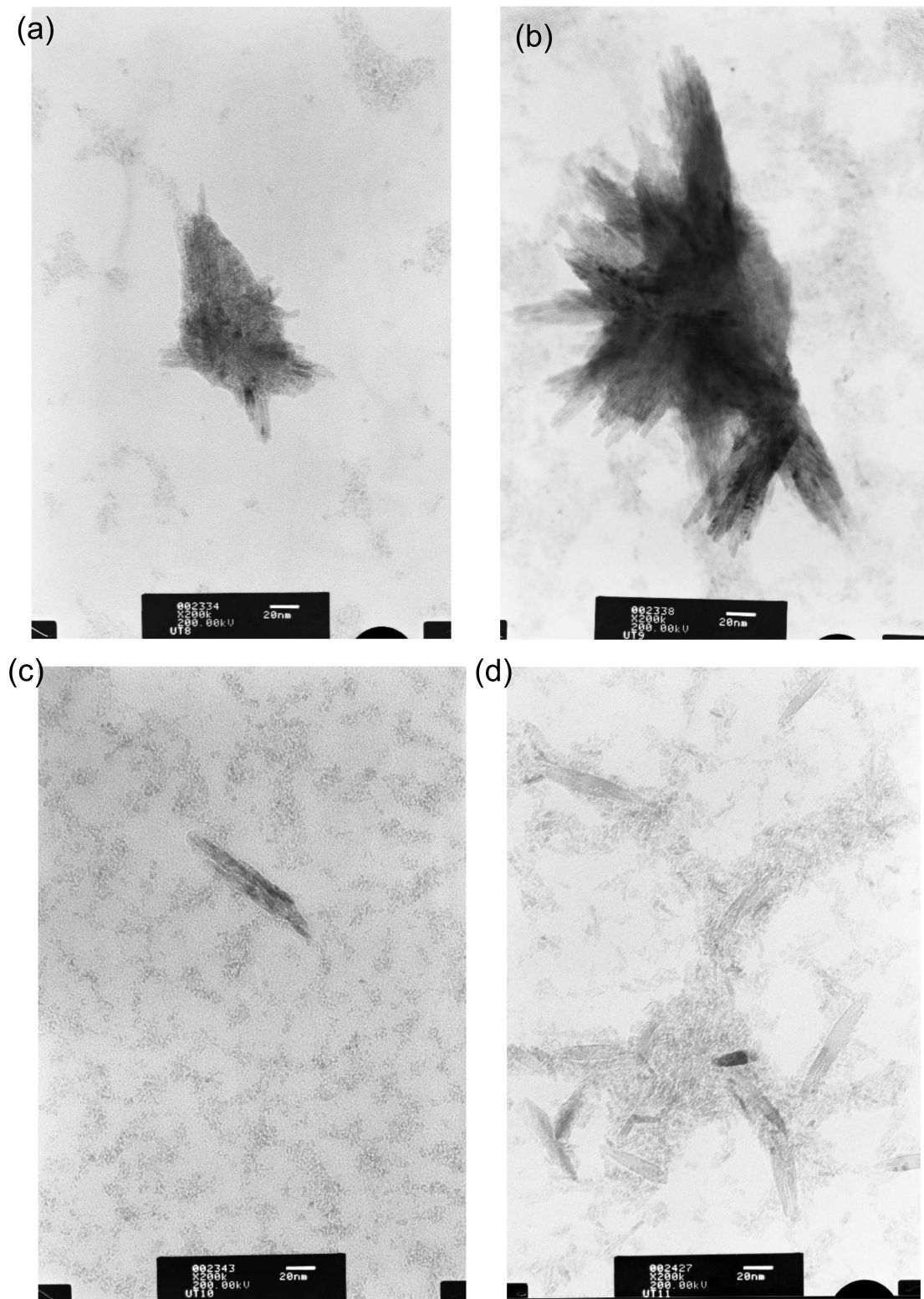


Figure 9. Cont.

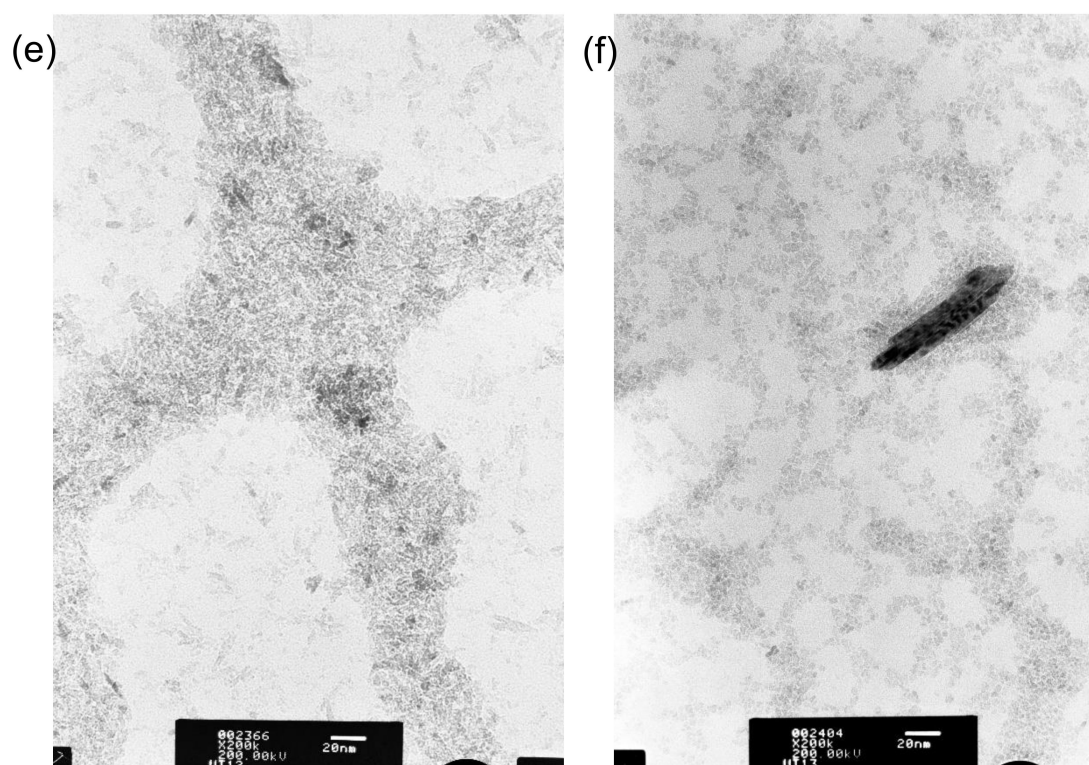


Figure 9. TEM images of particles obtained with 1.37 M TiCl_4 (with respect to the aqueous phase) and 1 wt % Span 80 (with respect to the oil) in hexadecane. The emulsification was performed with Ultra Turrax. In cases (a–c), the initial emulsions were prepared at 20,500 rpm for 5 min and the emulsion mixing was made at (a) 8000 rpm, (b) 13,500 rpm, and (c) 20,500 rpm for 10 min. In cases (d–f) the initial emulsions were obtained at (d) 8000 rpm, (e) 13,500 rpm and (f) 20,500 rpm, while the emulsion mixing was made at 20,500 rpm for 10 min.

Independent X-ray analysis of the dried TiO_2 particles showed that they have the crystal structure of anatase and rutile, Figure 10. In Figure 10b, we see that the predominant fraction of the obtained particles is of anatase crystal structure.

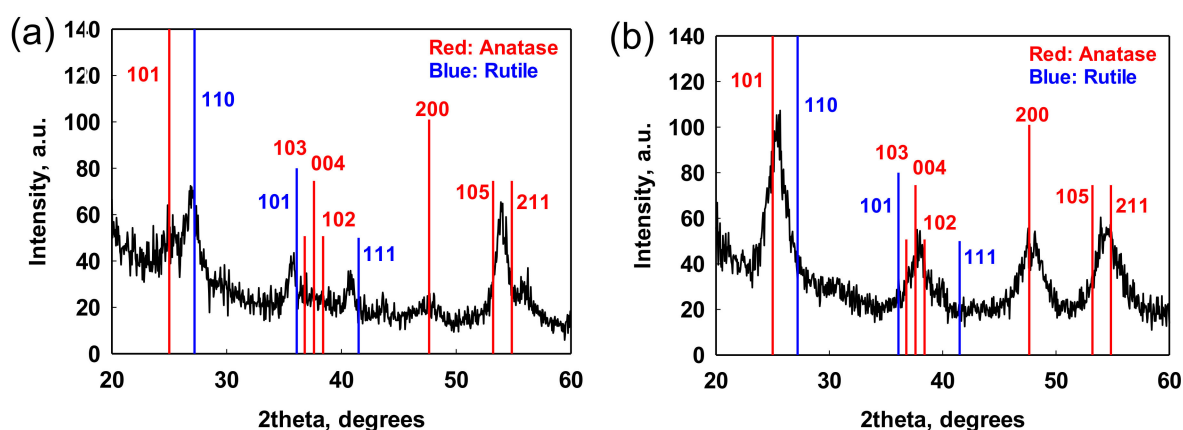


Figure 10. Data from the X-ray analysis of the dried particles, synthesized in emulsions which were obtained by Ultra Turrax stirring at (a) 20,500 rpm for 20 min and (b) 8000 rpm for 15 min. The initial emulsions were obtained by stirring at 20,500 rpm for 5 min. 1 wt % Span 80 in hexadecane was used as oily phase in both experiments.

4. Conclusions

In the current study, we show that the two-emulsion method can be used to obtain TiO₂ particles and particulate aggregates of relatively high concentration of ca. 11 wt % with respect to the aqueous phase and ca. 1.6 wt % with respect to the final emulsion.

Preliminary screening showed that Span 80 with concentration in the range between 0.1 and 1 wt % in the oily phase (hexadecane or mineral oil) can be used as appropriate surfactant for stabilization of the initial W/O emulsions, containing the two reactants, TiCl₄ and NH₄OH. The TiO₂ aggregates can be obtained with different sizes, shapes and morphologies by varying several key operational parameters, such as the precursor concentration, viscosity of the oily phase, and the homogenization speed during the emulsification and/or during the emulsion mixing. Spherical capsules or bulky agglomerates of micrometer size with smooth or rough surfaces could be obtained by this method.

The experimental results show that the shapes of the obtained particulate aggregates depend strongly on the size of the primary particles which, in their turn, are determined by the conditions of the emulsion processing. Working with oil of low viscosity and at high precursor and surfactant concentrations, one can obtain spherical TiO₂ capsules with very smooth surface, which are composed of very small primary particles with size falling in the range of 1 to 5 nm. The increase of the viscosity of the oily phase or decrease of the precursor or surfactant concentration leads to the formation of bigger primary particles which aggregate into bulky micrometer-sized agglomerates with rough surfaces.

Several types of factors are involved in the preparation of such TiO₂ aggregates of various sizes and shapes. On one hand, the rate of drop–drop coalescence during the emulsion homogenization is affected by the surfactant concentration, oil viscosity, homogenization speed and time. On its turn, the rate of drop coalescence determines the volume in which the particles synthesis occurs. On the other hand, the concentrations of the precursor and of the formed byproduct affect the processes of particle nucleation and growth. Appropriate combination of conditions should be used to obtain TiO₂ primary particles and their aggregates of desired shape and size.

Supplementary Materials: The following are available online at <http://www.mdpi.com/2504-5377/4/4/57/s1>, Table S1: Surfactants tested for stabilizing W/O emulsion with Hexadecane and Heavy mineral oil; Figure S1: Mean diameter by number, dN, and by volume, dV, of the particles aggregates (a) before and (b) after drying at 120 °C as a function of concentration of Span 80 dissolved in Hexadecane. The measurements are performed by DLS method for particles obtained by twoemulsion method using Ultra Turrax at 13,500 rpm; Figure S2: Mean diameters by volume, dV, and by number, dN, as measured by DLS obtained from emulsions with Hexadecane and Heavy oil. Empty symbols and dashed lines correspond to measurements before drying of the particles and the full symbols and straight lines—after drying. The concentration of the surfactant with respect to the oil was 1 wt % Span 80. The emulsification was performed with Ultra Turrax at 20,500 rpm for 5 min for the initial emulsions and for 10 min for the mixed ones; Figure S3: Dependence of the particles' diameter as a function of mixing time for two different fixed rpms. The homogenization of the initial emulsions was performed for 5 min at 20,500 rpm. 1 wt % Span 80 in Hexadecane was used as oily phase.

Author Contributions: Conceptualization and methodology: S.S.T., N.D.D., and T.D.; Investigation: N.I.P.-B. and S.R.T.-G.; Writing—original draft preparation: N.I.P.-B.; Writing—review and editing: S.S.T., N.D.D., and T.D.; Supervision and project administration: S.S.T. and N.D.D. All authors have read and agreed to the published version of the manuscript.

Funding: This work was supported also by BASF, Ludwigshafen, Germany.

Acknowledgments: Nadya Politova-Brinkova acknowledges the financial support received from the program “Young scientists and Postdoctoral candidates” of the Bulgarian Ministry of Education and Science, MCD no. 577/17.08.2018.

Conflicts of Interest: The authors declare no conflict of interest.

References

1. Tsang, C.H.A.; Li, K.; Zeng, Y.; Zhao, W.; Zhang, T.; Zhan, Y.; Xie, R.; Leung, D.Y.C.; Huang, H. Titanium oxide based photocatalytic materials development and their role of in the air pollutants degradation: Overview and forecast. *Environ. Int.* **2019**, *125*, 200–228. [[CrossRef](#)] [[PubMed](#)]
2. Petronella, F.; Truppi, A.; Dell'Edera, M.; Agostiano, A.; Curri, M.L.; Comparelli, R. Scalable synthesis of mesoporous TiO₂ for environmental photocatalytic applications. *Materials* **2019**, *12*, 1853. [[CrossRef](#)] [[PubMed](#)]
3. Wang, Z.; Tong, Y.; Dang, L.; Gao, F.; Lu, Q. Templated synthesis of titanium dioxide tube-in-tube superstructures with enhanced photocatalytic and lithium storage performance. *Chem. Eng. J.* **2019**, *370*, 1434–1439. [[CrossRef](#)]
4. Lai, C.; Zhou, X.; Huang, D.; Zeng, G.; Cheng, M.; Qin, L.; Yi, H.; Zhang, C.; Xu, P.; Zhou, C.; et al. A review of titanium dioxide and its highlighted application in molecular imprinting technology in environment. *J. Taiwan Inst. Chem. Eng.* **2018**, *91*, 517–531. [[CrossRef](#)]
5. Wu, W.Q.; Xu, Y.F.; Liao, J.F.; Wang, L.; Kuang, D.B. Branched titania nanostructures for efficient energy conversion and storage: A review on design strategies, structural merits and multifunctionalities. *Nano Energy* **2019**, *62*, 791–809. [[CrossRef](#)]
6. Li, Y.F.; Liu, Z.P. Particle size, shape and activity for photocatalysis on titania anatase nanoparticles in aqueous surroundings. *J. Am. Chem. Soc.* **2011**, *133*, 15743–15752. [[CrossRef](#)]
7. Ramos-Delgado, N.A.; Gracia-Pinilla, M.; Mangalaraja, R.V.; O'Shea, K.; Dionysiou, D.D. Industrial synthesis and characterization of nanophotocatalysts materials: Titania. *Nanotechnol. Rev.* **2016**, *5*, 467–479. [[CrossRef](#)]
8. Wu, W.Q.; Feng, H.L.; Chen, H.Y.; Kuang, D.B.; Su, C.Y. Recent advances in hierarchical three-dimensional titanium dioxide nanotree arrays for high-performance solar cells. *J. Mater. Chem. A* **2017**, *5*, 12699–12717. [[CrossRef](#)]
9. Traversa, E. Design of ceramic materials for chemical sensors with novel properties. *J. Am. Ceram.* **1995**, *78*, 2625–2632. [[CrossRef](#)]
10. Kingon, A.I.; Maris, J.P.; Steiffer, S.K. Alternative dielectrics to silicon dioxide for memory and logic devices. *Nature* **2000**, *406*, 1032–1038. [[CrossRef](#)]
11. Narayanan, R.; Kwon, T.Y.; Kim, K.H. TiO₂ nanotubes from stirred glycerol/NH₄F electrolyte: Roughness, wetting behavior and adhesion for implant applications. *Mater. Chem. Phys.* **2009**, *117*, 460–464. [[CrossRef](#)]
12. Signoretto, M.; Ghedini, E.; Nichele, V.; Pinna, F.; Crocellà, V.; Cerrato, G. Effect of textural properties on the drug delivery behaviour of nanoporous TiO₂ matrices. *Microporous Mesoporous Mater.* **2011**, *139*, 189–196. [[CrossRef](#)]
13. Dong, H.; Tang, G.; Ma, T.; Cao, X. One-step fabrication of inorganic/organic hybrid microspheres with tunable surface texture for controlled drug release application. *J. Mater. Sci. Mater. Med.* **2016**, *27*, 1–8. [[CrossRef](#)] [[PubMed](#)]
14. Oh, S.; Jin, S. Titanium oxide nanotubes with controlled morphology for enhanced bone growth. *Mater. Sci. Eng. C* **2006**, *26*, 1301–1306. [[CrossRef](#)]
15. Zhang, H.; Banfield, J.F. Structural characteristics and mechanical and thermodynamic properties of nanocrystalline TiO₂. *Chem. Rev.* **2014**, *114*, 9613–9644. [[CrossRef](#)]
16. Lacroche, M.; Brohan, L.; Marchand, R.; Tournoux, M. New hollandite oxides: TiO₂(H) and K_{0.06} TiO₂. *J. Solid State Chem.* **1989**, *81*, 78–82. [[CrossRef](#)]
17. Dubrovinskaia, N.A.; Dubrovinsky, L.S.; Ahuja, R.; Prokopenko, V.B.; Dmitriev, V.; Weber, H.P.; Osorio-Guillen, J.M.; Johansson, B. Experimental and theoretical identification of a new high-pressure TiO₂ polymorph. *Phys. Rev. Lett.* **2001**, *87*, 275501. [[CrossRef](#)]
18. Dubrovinsky, L.S.; Dubrovinskaia, N.A.; Swamy, V.; Muscat, J.; Harrison, N.M.; Ahuja, R.; Holm, B.; Johansson, B. The hardest known oxide. *Nature* **2001**, *410*, 653–654. [[CrossRef](#)]
19. Akimoto, J.; Gotoh, Y.; Oosawa, Y.; Nonose, N.; Kumagai, T.; Aoki, K.; Takei, H. Topotactic Oxidation of Ramsdellite Li_{0.5}TiO₂, a New Polymorph of Titanium Dioxide: TiO₂(R). *J. Solid State Chem.* **1994**, *113*, 27–36. [[CrossRef](#)]
20. Muller, U. *Inorganic Structural Chemistry*, 2nd ed.; Wiley: Hoboken, NJ, USA, 1992.
21. Linsebigler, A.L.; Lu, G.; Yates, J.T. Photocatalysis on TiO₂ surfaces: Principles, mechanisms, and selected results. *Chem. Rev.* **1995**, *95*, 735–758. [[CrossRef](#)]

22. Mo, S.-D.; Ching, W.Y. Electronic and optical properties of three phases of titanium dioxide: Rutile, anatase and brookite. *Phys. Rev. B* **1995**, *51*, 13023–13032. [[CrossRef](#)] [[PubMed](#)]
23. Thompson, T.L.; Yates, J.T. Surface Science Studies of the Photoactivation of TiO₂s New Photochemical Processes. *Chem. Rev.* **2006**, *106*, 4428–4453. [[CrossRef](#)] [[PubMed](#)]
24. Matsui, M.; Akaogi, M. Molecular dynamics simulation of the structural and physical properties of the four polymorphs of TiO₂. *Mol. Simul.* **1991**, *6*, 239–244. [[CrossRef](#)]
25. Navrotsky, A.; Kleppa, O.J. Enthalpy of the Anatase-Rutile Transformation. *J. Am. Ceram. Soc.* **1967**, *50*, 626. [[CrossRef](#)]
26. Jamieson, J.C.; Olinger, B. Pressure-temperature studies of anatase, brookite, rutile and TiO₂(II): A discussion. *Am. Mineral.* **1969**, *54*, 1477–1481.
27. Hu, Y.; Tsai, H.L.; Huang, C.L. Phase transformation of precipitated TiO₂ nanoparticles. *Mater. Sci. Eng. A* **2003**, *344*, 209–214. [[CrossRef](#)]
28. McQueen, R.G.; Jamieson, J.C.; Marsh, S.P. Shock-wave compression and x-ray studies of titanium dioxide. *Science* **1967**, *155*, 1401–1404. [[CrossRef](#)]
29. Simons, P.Y.; Datchile, F. The structure of TiO₂ II, a high-pressure phase of TiO₂. *Acta Crystallogr.* **1967**, *23*, 334–336. [[CrossRef](#)]
30. Zhang, H.; Banfield, J.F. Understanding polymorphic phase transformation behavior during growth of nanocrystalline aggregates: Insights from TiO₂. *J. Phys. Chem. B* **2000**, *104*, 3481–3487. [[CrossRef](#)]
31. Tanaka, K.; Capule, M.F.V.; Hisanaga, T. Effect of crystallinity of TiO₂ on its photocatalytic action. *Chem. Phys. Lett.* **1991**, *187*, 73–76. [[CrossRef](#)]
32. Maruska, H.P.; Ghosh, A.K. Photocatalytic decomposition of water at semiconductor electrodes. *Sol. Energy* **1978**, *20*, 443–458. [[CrossRef](#)]
33. Gerischer, H.; Heller, A. Photocatalytic Oxidation of Organic Molecules at TiO₂ Particles by Sunlight in Aerated Water. *J. Electrochem. Soc.* **1992**, *139*, 113–118. [[CrossRef](#)]
34. Bickley, R.I.; Gonzalez-Carreno, T.; Lees, J.S.; Palmisano, L.; Tilley, R.J.D. A structural investigation of titanium dioxide photocatalysts. *J. Solid State Chem.* **1991**, *92*, 178–190. [[CrossRef](#)]
35. Bacsá, R.R.; Kiwi, J. Effect of rutile phase on the photocatalytic properties of nanocrystalline titania during the degradation of p-coumaric acid. *Appl. Catal. B Environ.* **1998**, *16*, 19–29. [[CrossRef](#)]
36. Ohno, T.; Sarukawa, K.; Tokieda, K.; Matsumura, M. Morphology of a TiO₂ photocatalyst (Degussa, P-25) consisting of anatase and rutile crystalline phases. *J. Catal.* **2001**, *203*, 82–86. [[CrossRef](#)]
37. Zhang, Z.; Wang, C.-C.; Zakaria, R.; Ying, J.Y. Role of Particle Size in Nanocrystalline TiO₂-Based Photocatalysts. *J. Phys. Chem. B* **2002**, *102*, 10871–10878. [[CrossRef](#)]
38. Van Grieken, R.; Aguado, J.; López-Muñoz, M.J.; Marugán, J. Synthesis of size-controlled silica-supported TiO₂ photocatalysts. *J. Photochem. Photobiol. A Chem.* **2002**, *148*, 315–322. [[CrossRef](#)]
39. Anpo, M.; Shima, T.; Kodama, S.; Kubokawa, Y. Photocatalytic hydrogenation of CH₃CCH with H₂O on small-particle TiO₂: Size quantization effects and reaction intermediates. *J. Phys. Chem.* **1987**, *91*, 4305–4310. [[CrossRef](#)]
40. Ali, I.; Suhail, M.; Alothman, Z.A.; Alwarthan, A. Recent advances in syntheses, properties and applications of TiO₂ nanostructures. *RSC Adv.* **2018**, *8*, 30125–30147. [[CrossRef](#)]
41. Chen, X.; Mao, S.S. Titanium dioxide nanomaterials: Synthesis, properties, modifications and applications. *Chem. Rev.* **2007**, *107*, 2891–2959. [[CrossRef](#)]
42. Carp, O.; Huisman, C.L.; Reller, A. Photoinduced reactivity of titanium dioxide. *Prog. Solid State Chem.* **2004**, *32*, 33–177. [[CrossRef](#)]
43. Nasr, M.; Eid, C.; Habchi, R.; Miele, P.; Bechelany, M. Recent Progress on Titanium Dioxide Nanomaterials for Photocatalytic Applications. *ChemSusChem.* **2018**, *11*, 3023–3047. [[CrossRef](#)] [[PubMed](#)]
44. Ge, M.; Cai, J.; Iocozzia, J.; Cao, C.; Huang, J.; Zhang, X.; Shen, J.; Wang, S.; Zhang, S.; Zhang, K.Q.; et al. A review of TiO₂ nanostructured catalysts for sustainable H₂ generation. *Int. J. Hydrogen Energy* **2017**, *42*, 8418–8449. [[CrossRef](#)]
45. Sugimoto, T.; Okada, K.; Itoh, H. Synthetic of Uniform Spindle-Type Titania Particles by the Gel-Sol Method. *J. Colloid Interface Sci.* **1997**, *193*, 140–143. [[CrossRef](#)]
46. Sugimoto, T.; Zhou, X.; Muramatsu, A. Synthesis of uniform anatase TiO₂ nanoparticles by gel-sol method: 1. Solution chemistry of Ti(OH)_n(4-n)⁺ complexes. *J. Colloid Interface Sci.* **2002**, *252*, 339–346. [[CrossRef](#)]

47. Sugimoto, T.; Zhou, X.; Muramatsu, A. Synthesis of uniform anatase TiO₂ nanoparticles by gel-sol method. 3. Formation process and size control. *J. Colloid Interface Sci.* **2003**, *259*, 43–52. [[CrossRef](#)]
48. Sugimoto, T.; Zhou, X.; Muramatsu, A. Synthesis of uniform anatase TiO₂ nanoparticles by gel-sol method. 4. Shape control. *J. Colloid Interface Sci.* **2003**, *259*, 53–61. [[CrossRef](#)]
49. Djerdj, I.; Arçon, D.; Jagličić, Z.; Niederberger, M. Nonaqueous synthesis of metal oxide nanoparticles: Short review and doped titanium dioxide as case study for the preparation of transition metal-doped oxide nanoparticles. *J. Solid State Chem.* **2008**, *181*, 1571–1581. [[CrossRef](#)]
50. Niederberger, M.; Bartl, M.H.; Stucky, G.D. Benzyl alcohol and titanium tetrachloride—A versatile reaction system for the non-aqueous and low-temperature preparation of crystalline and luminescent titania nanoparticles. *Chem. Mater.* **2002**, *14*, 4364–4370. [[CrossRef](#)]
51. Wang, H.; Liu, P.; Cheng, X.; Shui, A.; Zeng, L. Effect of surfactants on synthesis of TiO₂ nano-particles by homogeneous precipitation method. *Powder Technol.* **2008**, *188*, 52–54. [[CrossRef](#)]
52. Li, Y.; Guo, Y.; Liu, Y. Synthesis of high purity TiO₂ nanoparticles from Ti(SO₄)₂ in presence of EDTA as complexing agent. *China Particuol.* **2008**, *3*, 240–242. [[CrossRef](#)]
53. Chae, S.Y.; Park, M.K.; Lee, S.K.; Kim, T.Y.; Kim, S.K.; Lee, W.I. Preparation of size-controlled TiO₂ nanoparticles and derivation of optically transparent photocatalytic films. *Chem. Mater.* **2003**, *15*, 3326–3331. [[CrossRef](#)]
54. Rehan, M.; Lai, X.; Kale, G.M. Hydrothermal synthesis of titanium dioxide nanoparticles studied employing in situ energy dispersive X-ray diffraction. *Cryst. Eng. Comm.* **2011**, *13*, 3725–3732. [[CrossRef](#)]
55. Vijayalakshmi, R.; Rajendran, V. Synthesis and characterization of nano-TiO₂ via different methods. *Arch. Appl. Sci. Res.* **2012**, *4*, 1183–1190. [[CrossRef](#)]
56. Li, G.L.; Wang, G.H. Synthesis of nanometer-sized TiO₂ particles by a microemulsion method. *Nanostruct. Mater.* **1999**, *11*, 663–668. [[CrossRef](#)]
57. Lin, J.; Lin, Y.; Liu, P.; Meziani, M.J.; Allard, L.F.; Sun, Y.P. Hot-fluid annealing for crystalline titanium dioxide nanoparticles in stable suspension. *J. Am. Chem. Soc.* **2002**, *124*, 11514–11518. [[CrossRef](#)] [[PubMed](#)]
58. Zhang, D.; Qi, L.; Ma, J.; Cheng, H. Formation of crystalline nanosized titania in inverse micelles at room temperature. *J. Mater. Chem.* **2002**, *12*, 3677–3680. [[CrossRef](#)]
59. DeBenedetti, B.; Vallauri, D.; Deorsola, F.A.; Martinez Garcia, M. Synthesis of TiO₂ nanospheres through microemulsion reactive precipitation. *J. Electroceram.* **2006**, *7*, 37–40. [[CrossRef](#)]
60. Chhabra, V.; Pillai, V.; Mishra, B.K.; Morrone, A.; Shah, D.O. Synthesis, Characterization, and Properties of Microemulsion-Mediated Nanophase TiO₂ Particles. *Langmuir* **1995**, *11*, 3307–3311. [[CrossRef](#)]
61. Hsieh, C.S.; Zhu, H.; Wei, T.Y.; Chung, Z.J.; Yang, W.D.; Ling, Y.H. Applying the experimental statistical method to deal the preparatory conditions of nanometric-sized TiO₂ powders from a two-emulsion process. *J. Eur. Ceram. Soc.* **2008**, *28*, 1177–1183. [[CrossRef](#)]
62. Bauer, W.; Tomandl, G. Preparation of spherical TiO₂ particles by an emulsion method using TiCl₄. *Ceram. Int.* **1994**, *20*, 189–193. [[CrossRef](#)]
63. Nabi, G.; Qurat-ul, A.; Khalid, N.R.; Tahir, M.B.; Rafique, M.; Rizwan, M.; Hussain, S.; Iqbal, T.; Majid, A. A Review on Novel Eco-Friendly Green Approach to Synthesis TiO₂ Nanoparticles Using Different Extracts. *J. Inorg. Organomet. Polym. Mater.* **2018**, *28*, 1552–1564. [[CrossRef](#)]
64. Thakur, B.K.; Kumar, A.; Kumar, D. Green synthesis of titanium dioxide nanoparticles using Azadirachta indica leaf extract and evaluation of their antibacterial activity. *South Afr. J. Bot.* **2019**, *124*, 223–227. [[CrossRef](#)]
65. Boppella, R.; Mohammadpour, A.; Illa, S.; Farsinezhad, S.; Basak, P.; Shankar, K.; Manorama, S.V. Hierarchical rutile TiO₂ aggregates: A high photonic strength material for optical and optoelectronic devices. *Acta Mater.* **2016**, *119*, 92–103. [[CrossRef](#)]
66. Pan, J.H.; Zhang, X.; Du, A.J.; Sun, D.D.; Leckie, J.O. Self-etching reconstruction of hierarchically mesoporous F-TiO₂ hollow microspherical photocatalyst for concurrent membrane water purification. *J. Am. Chem. Soc.* **2008**, *130*, 11256–11257. [[CrossRef](#)] [[PubMed](#)]
67. Koo, H.J.; Kim, Y.J.; Lee, Y.H.; Lee, W.I.; Kim, K.; Park, N.G. Nano-embossed hollow spherical TiO₂ as bifunctional material for high-efficiency dye-sensitized solar cells. *Adv. Mater.* **2008**, *20*, 195–199. [[CrossRef](#)]
68. Zheng, Z.; Huang, B.; Lu, J.; Qin, X.; Zhang, X.; Dai, Y. Hierarchical TiO₂ microspheres: Synergetic effect of {001} and {101} facets for enhanced photocatalytic activity. *Chem. A Eur. J.* **2011**, *17*, 15032–15038. [[CrossRef](#)]
69. Hu, X.; Zhang, T.; Jin, Z.; Huang, S.; Fang, M.; Wu, Y.; Zhang, L. Single-crystalline anatase TiO₂ dous assembled micro-sphere and their photocatalytic activity. *Cryst. Growth Des.* **2009**, *9*, 2324–2328. [[CrossRef](#)]

70. Yan, K.; Wu, G.; Jarvis, C.; Wen, J.; Chen, A. Facile synthesis of porous microspheres composed of TiO₂ nanorods with high photocatalytic activity for hydrogen production. *Appl. Catal. B Environ.* **2014**, *148–149*, 281–287. [[CrossRef](#)]
71. Ilaiyaraja, P.; Das, T.K.; Mocherla, P.S.V.; Sudakar, C. Well-connected microsphere-nanoparticulate TiO₂ composites as high performance photoanode for dye sensitized solar cell. *Sol. Energy Mater. Sol. Cells.* **2017**, *169*, 86–97. [[CrossRef](#)]
72. Yan, K.; Wu, G. Titanium Dioxide Microsphere-Derived Materials for Solar Fuel Hydrogen Generation. *ACS Sustain. Chem. Eng.* **2015**, *3*, 779–791. [[CrossRef](#)]
73. Yu, C.; Zhou, W.; Liu, H.; Liu, Y.; Dionysiou, D.D. Design and fabrication of microsphere photocatalysts for environmental purification and energy conversion. *Chem. Eng. J.* **2016**, *287*, 117–129. [[CrossRef](#)]
74. Jiao, Y.; Peng, C.; Guo, F.; Bao, Z.; Yang, J.; Schmidt-Mende, L.; Dunbar, R.; Qin, Y.; Deng, Z. Facile synthesis and photocatalysis of size-distributed TiO₂ hollow spheres consisting of {116} plane-oriented nanocrystallites. *J. Phys. Chem. C* **2011**, *115*, 6405–6409. [[CrossRef](#)]
75. Collins, A.M.; Spickermann, C.; Mann, S. Synthesis of titania hollow microspheres using non-aqueous emulsions. *J. Mater. Chem.* **2003**, *13*, 1112–1114. [[CrossRef](#)]
76. Lee, M.H.; Tai, C.Y.; Lu, C.H. Synthesis of spherical zirconia by precipitation between two water/oil emulsions. *J. Eur. Ceram. Soc.* **1999**, *19*, 2593–2603. [[CrossRef](#)]
77. Lee, J.S.; Lee, J.S.; Choi, S.C. Synthesis of nano-sized ceria powders by two-emulsion method using sodium hydroxide. *Mater. Lett.* **2005**, *59*, 395–398. [[CrossRef](#)]
78. Shi, J.; Verweij, H. Synthesis and purification of oxide nanoparticle dispersions by modified emulsion precipitation. *Langmuir* **2005**, *21*, 5570–5575. [[CrossRef](#)]
79. Tai, C.Y.; Lee, M.H.; Wu, Y.C. Control of zirconia particle size by using two-emulsion precipitation technique. *Chem. Eng. Sci.* **2001**, *56*, 2389–2398. [[CrossRef](#)]
80. Dolcet, P.; Maurizio, C.; Casarin, M.; Pandolfo, L.; Gialanella, S.; Badocco, D.; Pastore, P.; Speghini, A.; Gross, S. An effective two-emulsion approach to the synthesis of doped ZnS crystalline nanostructures. *Eur. J. Inorg. Chem.* **2015**, *2015*, 706–714. [[CrossRef](#)]
81. Yang, W.-D.; Hsieh, C.-S.; Wei, T.-Y.; Chung, Z.-J.; Huang, I.-L. Synthesis and Characterizations of Nanometric-Sized TiO₂ Powders as a Photocatalyst for Water Splitting. *J. Nanosci. Nanotechnol.* **2009**, *9*, 3843–3847. [[CrossRef](#)]

Publisher's Note: MDPI stays neutral with regard to jurisdictional claims in published maps and institutional affiliations.



© 2020 by the authors. Licensee MDPI, Basel, Switzerland. This article is an open access article distributed under the terms and conditions of the Creative Commons Attribution (CC BY) license (<http://creativecommons.org/licenses/by/4.0/>).